Limit equilibrium analyses of geosynthetic-reinforced two-tiered walls: Calibration from centrifuge tests

Suliman B.A. Mohamed [a,1], Kuo-Hsin Yang [a,*], Wen-Yi Hung [b,2]

[a] Department of Construction Engineering, National Taiwan University of Science and Technology, 43, Sec. 4, Keelung Rd., Taipei 106, Taiwan
[b] National Center for Research on Earthquake Engineering, 200, Sec. 3, Xinhai Rd., Taipei 10668, Taiwan

ARTICLE INFO

ABSTRACT

The use of limit equilibrium (LE) for predicting performance at failure in centrifuge two-tiered geo-synthetic-reinforced soil (GRS) wall models was evaluated. The variables considered in the centrifuge testing program were offset distance, D, and reinforcement length. Parametric studies were first per-formed to evaluate the effects of modeling assumptions of reinforcement force on LE results, including reinforcement force orientation, and reinforcement tensile load distribution with depth. The suitability of LE for the analysis of two-tiered GRS walls and design implications were then discussed. According to LE results, good agreement existed between LE and centrifuge models in locating failure surfaces. The LE results also indicate that offset distance correlated negatively with the effective overburden pressure on the reinforcement and the resulting confined T_{ult} of the reinforcement. The critical offset distance of 0.7 times the lower tier height was determined when the decrease in confined T_{ult} value as D increases reached a constant value. The LE analyses show that minimum reinforcement length of the upper tier ($L_{1,min} = 0.7H_1$), according to the compound design in FHWA design guidelines, is insufficient, such that failure surfaces do not pass through all reinforcement layers in the upper tier. Last, the effect of offset distance on the normalized reinforcement tension summation coefficient, K_T, indicates that single and independent wall models yielded a single consistent K_T value. For compound wall models, the K_T value decreases as offset distance D increases.

© 2013 Elsevier Ltd. All rights reserved.

1. Introduction

Mechanically stabilized earth (MSE) retaining structures are utilized in tiered configurations for various reasons, including aesthetics, stability and construction constraints. A lateral earth pressure method is widely used when designing these retaining structures (Elias et al., 2001; Berg et al., 2009; NCMA, 2010). The earth pressure method for designing multi-tiered reinforced walls is an extension of the design method for single-tiered reinforced walls. Some studies, however, have questioned the use of this empirical approach (Leshchinsky and Han, 2004). Very few studies have confirmed that the earth pressure method is effective for designing multi-tiered reinforced walls, and few have investigated the behavior and performance of geosynthetic-reinforced soil (GRS) walls in a tiered configuration.

Stuedlein et al. (2010) characterized the design and reported monitoring data for a four-tier 46 m tall wall reinforced with ribbed steel strips. Liu et al. (2012) acquired extensive field observations and applied numerical analyses to examine the failure mechanism and causes contributing to failures of a high steep multi-tiered geogrid-reinforced slope under heavy rainfall and earthquake. Yoo and Jung (2004) and Yoo and Kim (2008) investigated the performance and behavior of full-scale two-tiered GRS walls. Reduced-scale and centrifuge wall models have been used to characterize the internal stability of two-tiered GRS walls with varying offset distances (Yoo et al., 2011; Hung, 2008). The perfor-mance and stability of multi-tiered GRS structures under static (Leshchinsky and Han, 2004; Osborne and Wright, 2004; Wright, 2005; Yoo and Song, 2007; Yoo and Kim, 2008; Stuedlein et al., 2010; Yoo et al., 2011) and seismic loading conditions (Liu, 2011) have also been analyzed numerically. Current design approaches for multi-tiered reinforced walls and related research findings are discussed in the next section.

Notably, current FHWA design guidelines (Elias et al., 2001; Berg et al., 2009) recommend using the lateral earth pressure method when designing reinforced walls (e.g., single or multi-tiered walls)

and the limit equilibrium (LE) method when designing reinforced slopes. Walls and slopes are differentiated by a facing inclination of 70°. However, this face inclination is an arbitrary limitation because no reason exists why the LE method is not theoretically applicable to design reinforced walls. Further, because global and compound stabilities of reinforced walls must be ensured by slope stability analyses, it would be more convenient and straightforward for internal stability design of reinforced walls using LE method as well. Wright (2005), based on the results of limit equilibrium analyses, developed a series of design charts for design of tiered MSE walls. In addition, a comparison of finite difference and LE analyses by Leshchinsky and Han (2004) confirmed that LE analyses can be applicable for analyzing multi-tiered walls. However, to date, LE performance predictions at failure of multi-tiered GRS walls have not been fully validated in physical models.

These shortcomings prompted the current LE analyses of centrifuge two-tiered GRS wall models with varying offset distances, D. The objectives of this study are twofold: first, to evaluate the validity of LE in analyzing and designing multi-tiered GRS walls, and second, to examine the current design methods for multi-tiered GRS walls by referencing the results of centrifuge tests and limit equilibrium analyses. Thus, experimental results and LE predictions were compared, specifically for failure surface locations. This study also examined the influence of offset distance on the confined (or in-soil) T_{ult} of the reinforcement. The confined T_{ult} was back-calculated from LE analyses at failure in centrifuge wall models (i.e., FS = 1.0). The influence of offset distance on the reinforcement can be interpreted as the influence of offset distance on effective overburden pressure and the resulting confined T_{ult}. A critical offset distance beyond which the two tiers act independently can therefore be determined when the confined T_{ult} reaches a constant value. The effect of reinforcement length on the centrifuge test and LE results was also evaluated. Finally, normalized centrifuge test results and design implications for multi-tiered GRS walls are discussed.

2. Current design approach and related research findings

Design of multi-tiered MSE walls is addressed by FHWA (Elias et al., 2001; Berg et al., 2009) and NCMA (2010) design guidelines. The FHWA and NCMA design approaches are limited to two-tiered walls, but suggest that their design approaches can be extended to walls with more than two tiers by considering an additional vertical stress due to the effect of overlying wall tiers. The design approaches in these guidelines are considered empirical and geometrically derived based on the relative distance or offset distance between upper and lower tiers. Fig. 1 illustrates the methods used to determine maximum tension lines, defined as internal failure surfaces, and additional vertical stresses for the internal stability analysis in FHWA design guidelines. For cases with a small offset distance, $D \leq (H_1 + H_2)/20$, where H_1 and H_2 are the height of upper and lower tiers, respectively, two tiers are designed as a single wall (Fig. 1-a1) with the same failure plane as that of a wall with a height of $H = H_1 + H_2$. The minimum reinforcement lengths for the upper and lower tiers should be $L_{1,min} = L_{2,min} = 0.7(H_1 + H_2)$. For cases with intermediate offset distances, $(H_1 + H_2)/20 < D \leq \tan(45° - \phi/2)H_2$, where ϕ is the internal friction angle of backfill, two tiers are designed as a compound wall (Fig. 1-a2). The location of the failure plane varies with offset distance, and minimum reinforcement lengths are $L_{1,min} = 0.7H_1$ and $L_{2,min} = 0.6(H_1 + H_2)$. Notably, when offset distance is within the range of $\tan(45° - \phi/2) H_2 < D \leq \tan(90° - \phi)H_2$, failure surfaces develop separately in the upper and lower tiers (Fig. 1-a3), but the additional vertical stress from the upper tier still affects reinforcements in the lower tier. Therefore, the two tiers are still designed as a compound wall. For

cases with a large offset distance, $D > \tan(90° - \phi)H_2$, two tiers are not considered superimposed when one assumes no interaction exists between the two tiers and they are designed as two independent walls. Failure planes may develop for the upper and lower tiers separately, with minimum reinforcement lengths of $L_{1,min} = 0.7H_1$ and $L_{2,min} = 0.7H_2$.

In the NCMA design guidelines, the two tiers are considered independent when offset distance exceeds reinforcement length of the lower tier needed in internal stability or beyond the failure surface in external analysis; otherwise, the upper tier is taken as an equivalent uniform surcharge affecting the lower tier. The magnitude of the equivalent uniform surcharge is function of D and H_1 based on linear interpolation between single and independent wall cases. Design procedure details are presented in NCMA guidelines (2010).

Hung (2008) conducted a series of centrifuge model tests to investigate the internal failure mechanism of single and two-tier GRS walls. Hung found that when reinforced walls with $(H_1 + H_2)/20 \leq D \leq (H_1 + H_2)/6.8$ are designed as a compound wall in accordance with FHWA design guidelines, the upper tier is likely unstable due to insufficient L_1, per FHWA design guidelines. Consequently, Hung suggested that the two-tier walls should be designed as a single wall when $D \leq (H_1 + H_2)/6.8$. When $D > \tan(45° - \phi/2)H_2$, the failure surfaces in the two tiers developed separately. Hung also observed that the failure plane with an angle of $\theta = (\beta + \phi)/2$, where β is equivalent wall inclination (Fig. 1), can encompass the experimental failure surfaces in centrifuge tests.

Yoo et al. (2011) assessed the internal stability of two-tiered GRS walls using reduced-scale physical models and finite element (FE) simulations. Both physical and FE results identify internal failure patterns in relation to offset distance. These independent failure surfaces developed in the upper and lower tiers when $D > 0.7H_2$. The critical offset distance was $D_{cr} = 0.8H_2$ by FE simulation when the increase in the factor of safety (FS) and the increase in D reached a constant value. The D_{cr} value determined by Yoo et al. (2011) is almost half that in FHWA design guidelines. The FE results of a parametric study by Yoo et al. (2011) demonstrated that reinforcement length of the lower tier has a greater impact on the wall stability than that of the upper tier. They suggested that minimum reinforcement lengths are $L_{1,min} = 0.75H_1$ and $L_{2,min} = 0.7H_2$ for independent wall design and $L_{1,min} = 1.25H_1$ and $L_{2,min} = 0.9H_2$ for compound wall design.

Leshchinsky and Han (2004) analyzed multi-tier walls numerically. They found that an increase in offset distance reduced the required tensile strength of the reinforcement. The D_{cr} was determined using LE analysis when the decrease in required tensile strength of the reinforcement with the increase in D reached a constant value. The D_{cr} value was a function of backfill quality, 0.8–1.2 times individual tier height for backfill with a ϕ of 34°−25°. The effect of reinforcement length depended on the height and offset distance of multi-tiered walls and backfill quality. Notably, Leshchinsky and Han (2004) found that LE analysis (ReSSA v.2.0) of multi-tiered walls yielded nearly the same FS as continuum mechanics-based analysis (FLAC 2D). Therefore, they concluded that LE analyses are applicable for analyzing multi-tiered walls.

3. Centrifuge tests and limit equilibrium analyses

3.1. Centrifuge tests

A series of centrifuge tests were conducted at the National Central University (NCU), Taiwan, to investigate performance and failure mechanisms in single and two-tiered GRS walls (Hung, 2008). To perform the LE analyses in the current study, a total of fourteen centrifuge model tests were selected from the Hung's
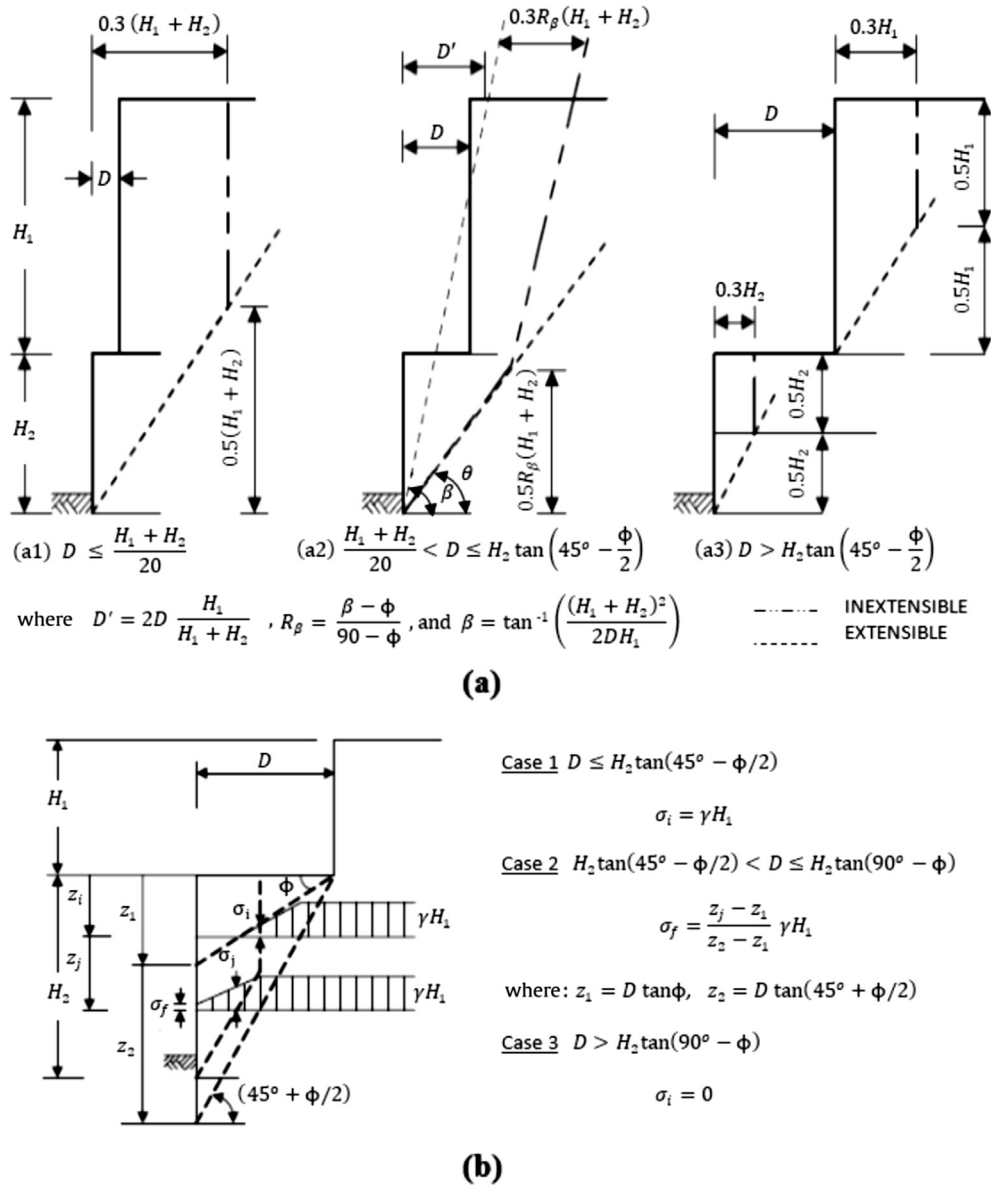
Fig. 1. FHWA design guidelines criteria for a two-tier MSE walls: (a) location of maximum tension lines; (b) additional vertical stress (after Elias et al., 2001).

centrifuge testing program. Centrifuge models were constructed in a rigid aluminum container with internal dimensions of 820 mm × 450 mm in plan × 580 mm in height. For all models, the wall heights of the upper and lower tiers were $H_1 = H_2 = 160$ mm, and additional layer of 20 mm of soil was deposited on the top of the upper tier to cover the topmost reinforcement layer. Therefore, the wall models have an equivalent height of 340 and were built on a foundation layer 150 mm thick. Fig. 2 shows a schematic profile and photo of the model wall. Each model was built using the same number of reinforcement layers: 9 for the upper tier and 8 for the lower with 20 mm vertical spacing. Except for the topmost reinforcement, each reinforcement layer was folded back at the face of the wall models, forming a wrap-around facing and a secondary (overlapping) layer ($L_0 = 40\%$ of reinforcement length for each tier).

In all centrifuge models, offset distance D ranged from 0 mm to 270 mm. Table 1 summarizes the geometrical configuration, reinforcement length and test results for the two-tiered GRS wall models. The wall models were grouped into four test series (S, C, I, and SR):

(1) Single (S) series: two wall models were single wall designs with $D \leq (H_1 + H_2)/20$ and $L_1 = L_2 = 0.7(H_1 + H_2)$ (i.e., $D \leq 16$ mm and $L_1 = L_2 = 224$ mm).

(2) Compound (C) series: eight wall models were compound wall designs with $(H_1 + H_2)/20 < D \leq \tan(90° - \phi)H_2$ and $L_1 = L_2 = 0.6(H_1 + H_2)$ (i.e., 16 mm $< D \leq 194$ mm and $L_1 = L_2 = 192$ mm). Notably, the selected L_1 is longer than the minimum reinforcement length (i.e., $L_1 = 0.7H_1$) for compound wall design recommended in FHWA design guidelines to prevent the instability of the upper tier during testing.

(3) Independent (I) series: two wall models were independent wall designs with $D > \tan(90° - \phi)H_2$, $L_1 = 0.7H_1$ and $L_2 = 0.7H_2$ (i.e., $D > 194$ mm and $L_1 = L_2 = 112$ mm).

(4) Shorter Reinforcement (SR) series: two wall models were compound wall designs with $(H_1 + H_2)/20 < D \leq \tan(90° - \phi)$ H_2, $L_1 = 0.7H_1$ and $L_2 = 0.6(H_1 + H_2)$ (i.e., 16 mm $< D \leq 194$ mm, $L_1 = 112$ mm and $L_2 = 192$ mm). The reinforcement length of upper tier is in accordance with the minimum reinforcement length in FHWA design guidelines.
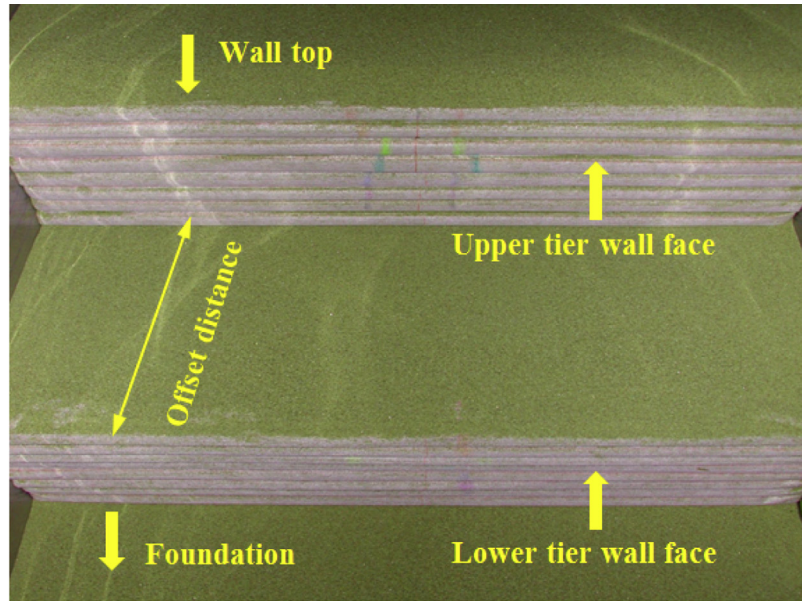
(a)
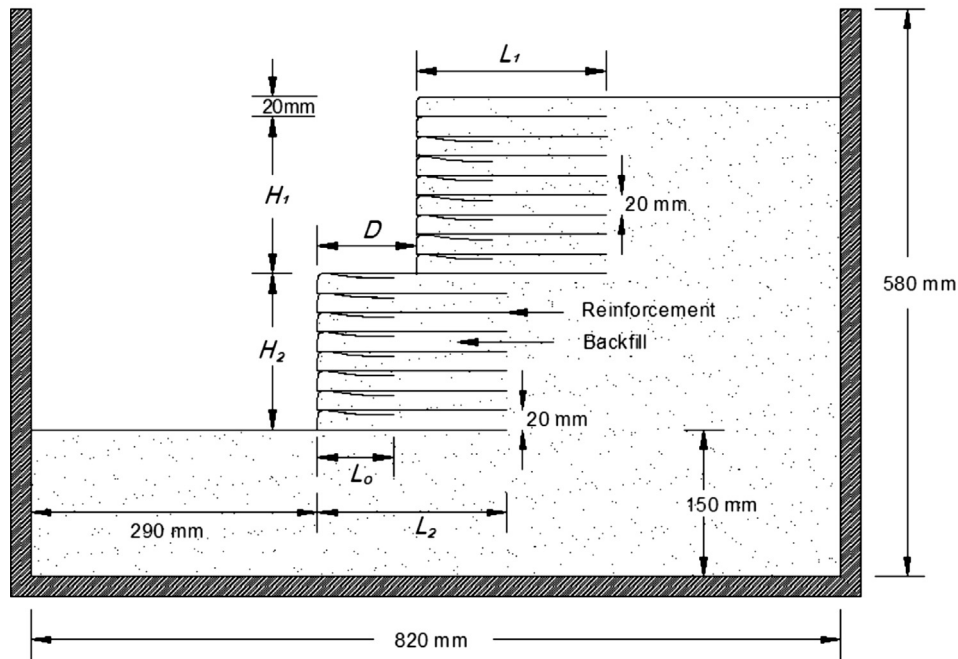
(b)

Fig. 2. Configuration of a centrifuge two-tiered GRS wall model: (a) front view of model after construction completion; (b) schematic profile view of model (D is the offset distance; L_1 and L_2 are the reinforcement length of the upper and lower tiers; L_o is the overlap length of reinforcement).

The centrifuge testing procedure was divided into two stages. In the first stage, the model wall was supported by a wooden form-work and flew to 40 g until the measured settlement at the top of the wall was stable (to compress any voids through increasing self-weight) and then decelerated to a complete stop. In the second stage, the wooden formwork was removed and the models were loaded by gradually increasing the centrifuge acceleration in increments of 2 g until the model failed. Each level of acceleration was maintained for 30 s. Two CCD cameras recorded the wall deformation during the tests. One was positioned in front of the side view window of the container, and the other was placed on the top of the container.

Table 1 summarizes the failure g-level, N_f, recorded for each model. Fig. 3 shows the initial and failure conditions observed in

Table 1
Geometrical configurations and test results of two-tiered GRS wall models.

Test No.		Wall parameters			Reinforcement length		Results	
		D (mm)	θ (deg.)	β (deg.)	L_1 (mm)	L_2 (mm)	N_f (g)	Back-calculated T_{ult} (kN/m)
S-series	1	0	59.0	90	224	224	16	0.115
	2	10	57.8	88.2	224	224	18	0.123
C-series	3	20	56.4	86.4	192	192	16	0.105
	4	30	55.1	84.7	192	192	18	0.112
	5	40	53.6	82.9	192	192	16	0.092
	6	50	52.1	81.1	192	192	18	0.098
	7	60	50.5	79.4	192	192	18	0.092
	8	70	48.9	77.7	192	192	19	0.092
	9	80	47.2	76.0	192	192	18	0.077
	10	90	45.5	74.3	192	192	18	0.069
I-series	11	260	59.0	90[a]	112	112	18/17[b]	0.076/0.063[b]
	12	270	59.0	90[a]	112	112	18/18[b]	0.076/0.066[b]
SR-series	13	20	56.4	86.4	112	192	15	0.120
	14	60	50.5	79.4	112	192	16	0.100

Note: D = Offset distance; θ = Failure plane angle in FHWA design guidelines; β = Equivalent wall inclination in FHWA design guidelines; L_1 = Reinforcement length of upper tier; L_2 = Reinforcement length of lower tier; N_f = Failure g-level of centrifuge model; T_{ult} = Back-calculated ultimate tensile strength of reinforcement.
[a] I-series is analyzed as two vertical single walls separately.
[b] Results for upper/lower tier.
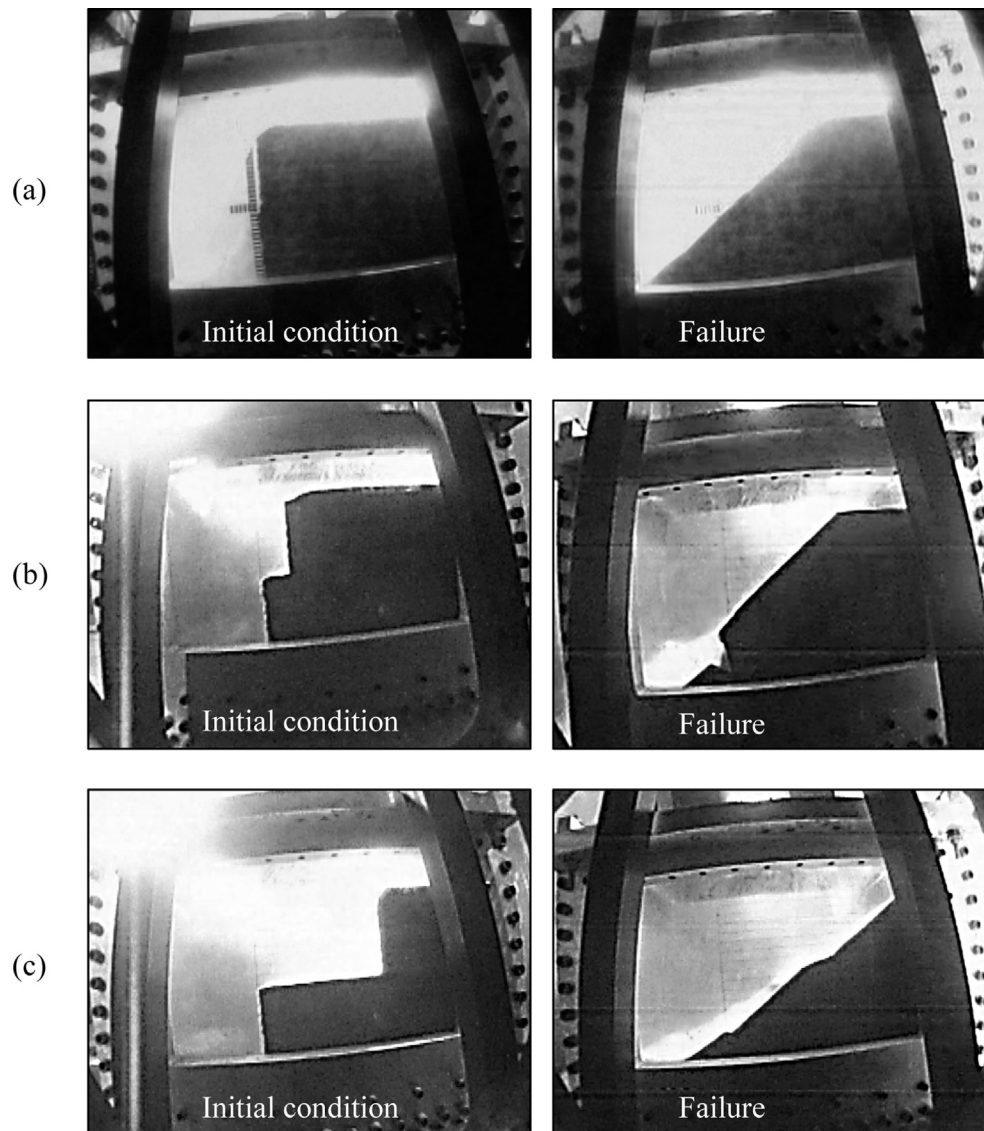
Fig. 3. Photos of centrifuge tests: (a) Test S2 (design as a single wall); (b) Test C4 (design as a compound wall); (c) Test I12 (design as an independent wall).
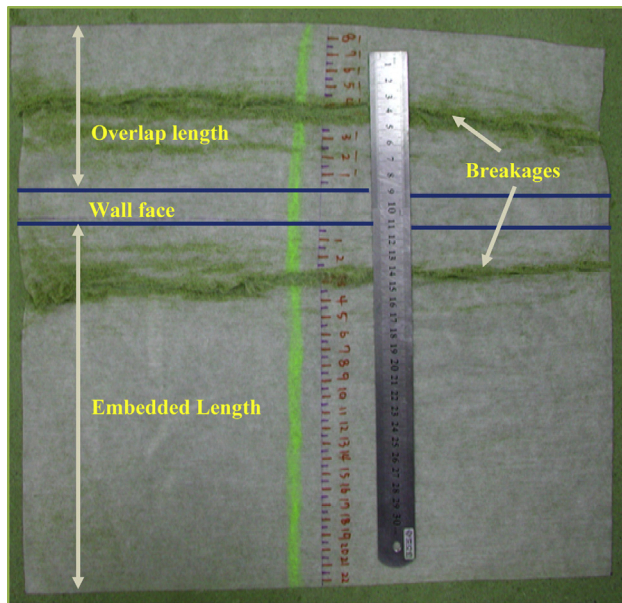
Fig. 4. Breakage pattern in reinforcement material after wall failure.

Fig. 5. Particle size distribution curve for sand backfill.

Test S2, C4, and I12. Fig. 4 shows a broken reinforcement carefully retrieved from the dismantled wall models after tests completed. The nearly horizontal breakage pattern in the reinforcement validates the plane strain condition in the centrifuge tests. The location of the critical failure surface was determined based on the observed tears (ruptures) in each layer of the reinforcement. The centrifuge testing program is discussed in further detail in Hung (2008).

3.2. Material properties

The soil used in the centrifuge test was clean and uniform Fulung beach sand, which is classified as poorly graded sand (SP) in the Unified Soil Classification System. Table 2 summarizes the properties of the Fulung sand used as the backfill and foundation material. Fig. 5 shows the particle size distribution curve for sand backfill. The backfill unit weight of sand and the friction angle obtained in a series of triaxial compression tests at the target relative density D_r of 70% were $\gamma = 15$ kN/m^3 and $\phi_{tx} = 39.5°$, respectively. To characterize the shear strength of the test sand under the plane strain condition in the centrifuge model, the plane strain peak friction angle ($\phi_{ps} = 42.3°$) was estimated using the correlation between the triaxial compression friction angle and the plane strain friction angle (Lade and Lee, 1976):

$$\phi_{ps} = 1.5\phi_{tx} - 17 \qquad (1)$$

Table 2
Properties of the Fulung sand.

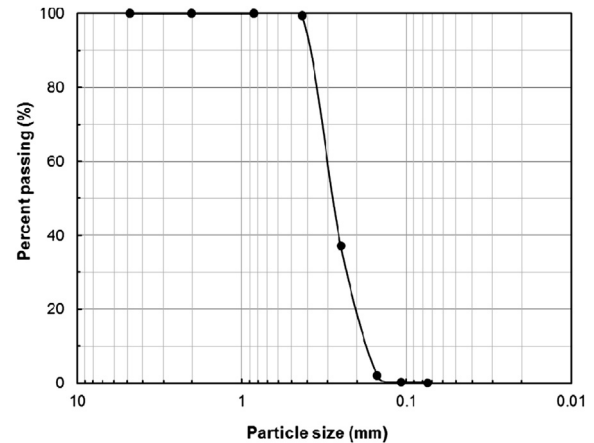| Property	Value
Specific gravity, G_s	2.66
Effective size, D_{10} (mm)	0.17
Average size, D_{50} (mm)	0.28
Coefficient of curvature, C_c	1.05
Coefficient of uniformity, C_u	1.78
Maximum dry unit weight, $\gamma_{d,max}$ (kN/m^3)	15.9
Minimum dry unit weight, $\gamma_{d,min}$ (kN/m^3)	13.3
Unit weight, γ (kN/m^3)	15.0
Triaxial compression friction angle, ϕ_{tx} (degree)	39.5
Plane strain friction angle, ϕ_{ps} (degree)	42.3

The geotextile used in the centrifuge study was nonwoven polyester, rayon fabric. A series of unconfined wide-width tensile tests (ASTM D4595) and zero-span tests with clamps 6 mm apart (Porbaha and Goodings, 1996) were performed to evaluate the strength properties of the geotextile material. The average T_{ult} for the geotextile were 0.05 kN/m from wide-width tests and 0.12 kN/m from zero-span test. As the nonwoven geotextile tensile strengths were found to be affected by soil confinement and impregnation of geotextile by soil particles (Boyle et al., 1996), unconfined tensile tests like wide-width and zero-span tensile tests may not accurately represent in-soil tensile strength values. However, experimentally quantifying the in-soil mechanical properties of low strength nonwoven fabrics is difficult. This study therefore performed a back analysis to calculate the confined ultimate tensile strength T_{ult} of reinforcement. Table 1 summarizes the confined T_{ult} values. The back analyses used to obtain the values for confined T_{ult} are discussed in Section 3.3.

3.3. Limit equilibrium analyses

Limit equilibrium analyses are typically used to analyze the stability of natural and reinforced slopes. Zornberg et al. (1998b) conducted a series of LE analyses of centrifuge GRS slope tests and demonstrated that LE is effective for predicting failure in GRS slopes. Nevertheless, the LE predictions of performance at failure in multi-tiered GRS walls have not been fully validated in physical models. In the current study, the LE calculations were performed using Spencer's method (Spencer, 1967) as coded in the Slide v.6.0 program. The Spencer's method, which is sufficiently rigorous to satisfy all equilibrium conditions, assumes that all inter slice forces are parallel. Both circular and noncircular failure surfaces are considered in this study. The non-circular failure surface comprised several piecewise linear segments, which were automatically generated by the program depending on the user-specified segment length. The search for the noncircular critical failure surface was initiated by specifying the locations of the first and last points of the initial failure surface. In modeling the S-, C- and SR-series, the first point on the initial failure surface was fixed near the toe of the lower-tier wall, and the last point was allowed to move along the top of the upper-tier wall. Failure surfaces developed separately in the upper and lower tiers in the centrifuge wall models of the I-series; thus, two critical failure surfaces were separately searched for each tier.

The shear strength of the test sand in the centrifuge model was characterized by the plane strain friction angle. The geotextile was modeled as a reinforcement element by inputting a tensile strength

value and a coverage ratio of 100%. The reinforcement–soil interface was assumed fully bonded by inputting high interface shear strength properties in the LE analyses. The LE analyses considered the contribution of geotextile overlap layers to system stability by modeling these overlap layers as additional reinforcement layers. Centrifugal force was simulated by increasing the unit weight of backfill N_f times until it corresponded to the target g-level at failure.

The LE analyses in this study were performed by adjusting the input tensile strength of reinforcement until FS = 1.0 was reached. This estimate accounted for the confined T_{ult} of the reinforcement and was expected to equal the average in-soil reinforcement tension at the moment of failure. Finally, reduction factors such as creep, installation damage and degradation were excluded because the centrifuge model tests were meticulously constructed to ensure that no installation damage occurred. The test duration was also kept sufficiently short to avoid long-term behavior such as creep or degradation. Fig. 6 shows the LE modeling and output of Test C4 obtained from the Slide program.

4. Evaluation of modeling assumptions of reinforcement load in limit equilibrium analysis

In LE analysis of GRS structures, stabilizing forces from reinforcement loads are incorporated into the equilibrium equation at the "limit" state. However, due to the problem of statically indeterminate when incorporating reinforcements into LE analysis, modeling the reinforcement load, T_{max}, at each reinforcement layer requires assumptions and further verification. Thus, this study performed parametric studies to evaluate the effects of modeling assumptions for T_{max} on LE results, including reinforcement tensile load distribution with depth, and orientation of reinforcement forces.

4.1. Effect of reinforced tensile load distribution

The effect of the maximum reinforcement load, T_{max}, distribution with a depth below the top of two-tiered GRS walls was investigated using LE analysis by assuming uniform, triangular (or linear), and multi-linear (or trapezoidal) distribution functions
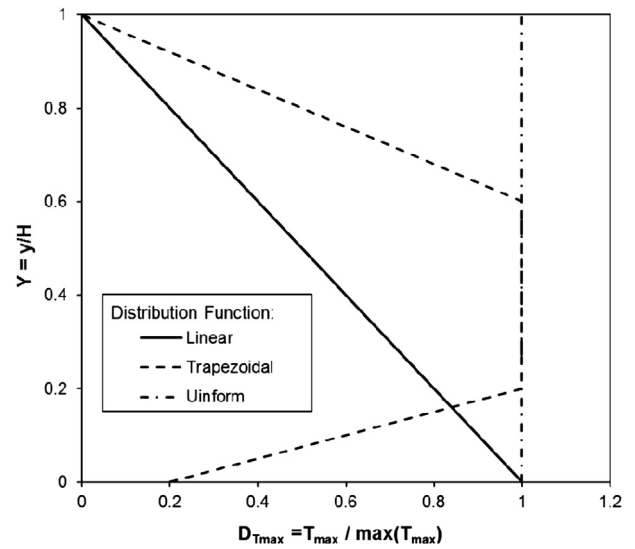

Fig. 7. Assumed reinforcement tensile force distribution functions (after Leshchinsky et al., 2010).

(Fig. 7). In Fig. 7, the distribution function D_{Tmax} is defined as the ratio of maximum mobilized force in each reinforcement layer, T_{max}, to maximum force of all reinforcement layers, max(T_{max}). The D_{Tmax} value reflects the normalized value of T_{max} as a function of the normalized elevation of $Y = y/H$.

These three distribution functions, uniform, triangular, and trapezoidal, were first used by Leshchinsky et al. (2010) to evaluate impact of assumed distribution functions on the required reinforcement strength in GRS single walls and slopes. A uniform distribution assumes all reinforcement layers reach their ultimate tensile strength simultaneously at the moment of failure (i.e., FS = 1.0). Zornberg et al. (1998b) used uniform distribution in LE analyses of centrifuge GRS slopes at failure. Their study showed very good agreement between failure g-levels and locations of failure surfaces obtained experimentally and those predicted by LE analysis, validating the assumption of uniform distribution. The linear
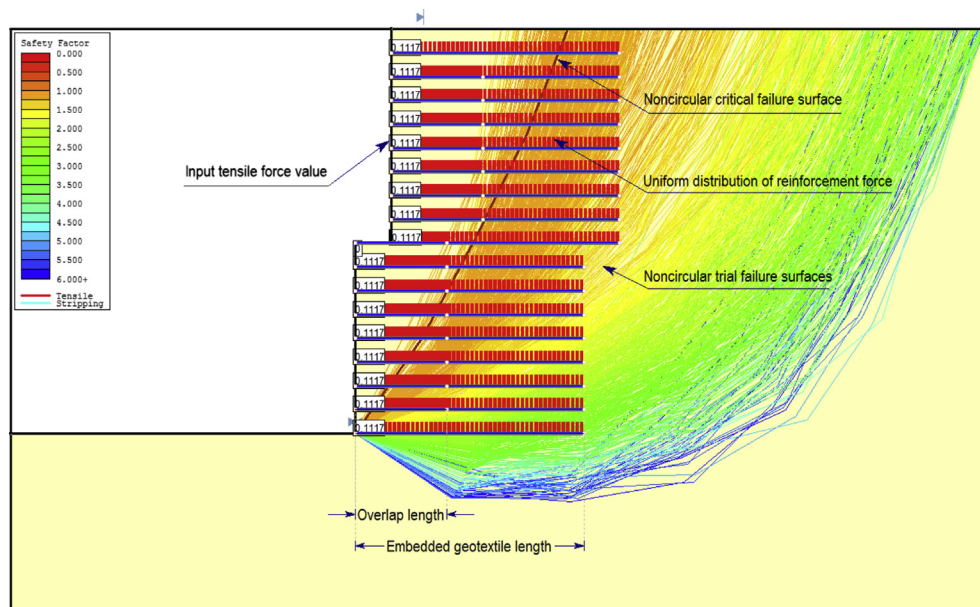

Fig. 6. Limit equilibrium modeling and output of Test C4 from the Slide program.
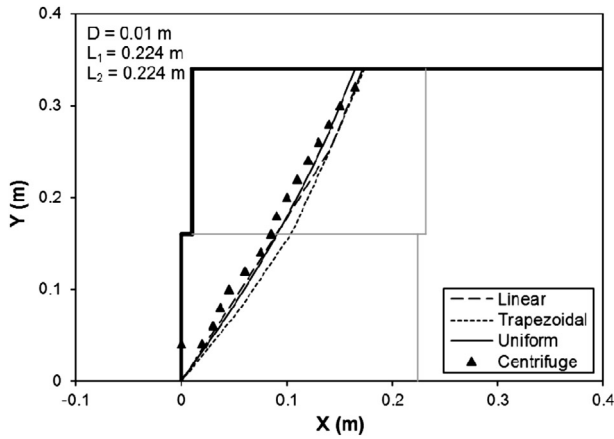
distribution assumes only the bottommost reinforcement layer reaches its ultimate tensile strength at the moment of failure. This linear distribution is assumed in current design charts for reinforced soil slopes, while considering that overburden pressure increases proportionally with depth below the slope (Schmertmann et al., 1987; Leshchinsky and Boedeker, 1989; Jewell, 1991). The trapezoidal distribution assumes only the middle of reinforcement layers reaches its ultimate tensile strength at the moment of failure. The

small mobilization of T_{max} at the upper and lower parts of walls is likely due to low overburden pressures at top areas and restrained wall deformation by the firm foundation at bottom areas, respectively. The trapezoidal function was based on empirical correlations in field data (Allen et al., 2003; Allen and Bathurst, 2002; Bathurst et al., 2008) and verified by FE results (Yang et al., 2012).
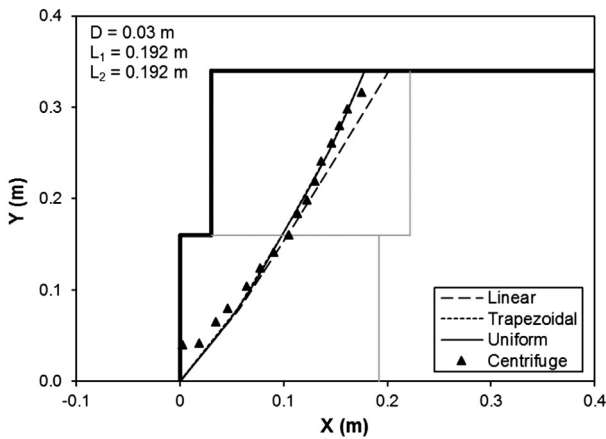
In this study, the LE calculated values of T_{max} for each reinforcement layer were assigned to each assumed distribution function and then determined iteratively until FS = 1.0. Fig. 8 shows the effect of the tensile load distribution on the predicted critical failure surfaces for Tests S2, C4, and I12. It can be seen that the predicted location of critical failure surface is insensitive to the assumed reinforcement load distribution. Fig. 9 presents the calculated T_{max} for each reinforcement layer in Test C4. The max(T_{max}) value obtained for the linear, trapezoidal, and uniform distributions is 0.188, 0.144, and 0.112 kN/m, respectively. The max(T_{max}) value obtained using the linear distribution is approximately 67% higher than the value obtained from the uniform distribution. The sum of T_{max} values for all reinforcement layers under linear, trapezoidal and uniform distributions is 1.7, 1.77, and 1.9 kN/m, respectively. The impact of the assumed D_{Tmax} on the sum of T_{max} values is small (<10% difference), implying that the system requires an equal total amount of resistance from reinforcements to maintain system equilibrium.

Table 3 summarizes the max(T_{max}) values obtained with the three assumed distributions and the T_{ult} values obtained from wide-width and zero-span tensile tests. The max(T_{max}) values obtained using the uniform distribution are lower than values obtained using linear and trapezoidal distributions (Table 3). The same conclusion was acquired by Leshchinsky et al. (2010) from LE results for two case examples of a GRS single wall and slope. Because the max(T_{max}) value is typically adopted to determine the required long-term strength of reinforcement, using the max(T_{max}) value from the uniform distribution can lead to a simple and cost-effective design.
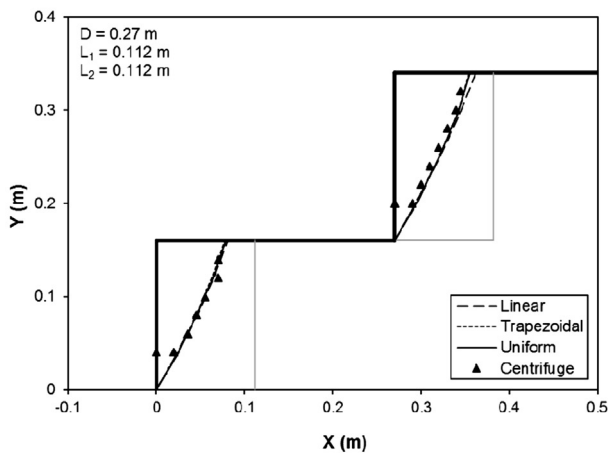
Moreover, the max(T_{max}) values obtained from back analysis using the uniform distribution are between the T_{ult} values obtained from the wide-width and zero-span tests. In single wall models, the max(T_{max}) values are close to the T_{ult} value obtained from the zero-span test. In compound models, the max(T_{max}) values decrease as offset distance increases. The max(T_{max}) values obtained from independent wall models are close to the T_{ult} value obtained from the wide-width test. It is important to note that the max(T_{max}) values in the single and compound wall models using linear and trapezoidal

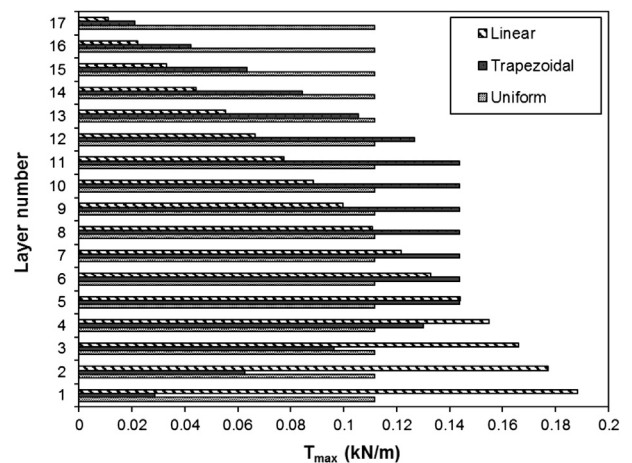**Fig. 8.** Effect of reinforcement tensile load distribution on predicted failure surface: (a) Test S2; (b) Test C4; (c) Test I12.

Fig. 9. Effect of reinforcement tensile load distribution on calculated T_{max} for each reinforcement layer in Test C4.

Table 3
Summary of max(T_{max}) values from the three assumed distributions for different wall models.

Design	Test No.	D (mm)	T_{ult} (kN/m)		max(T_{max}) (kN/m)		
			Wide-width	Zero-span	Linear	Trapezoidal	Uniform
Single	1	0	0.05	0.12	0.192	0.144	0.115
	2	10			0.205	0.154	0.123
Compound	4	30			0.188	0.144	0.112
	6	50			0.165	0.127	0.098
	7	60			0.158	0.117	0.092
Independent (upper/lower)	11	260			0.128/0.106	0.092/0.076	0.076/0.063
	12	270			0.128/0.112	0.092/0.080	0.076/0.066

distributions exceed the T_{ult} value obtained from zero-span test. These analytical results are questionable because many researchers (Christopher et al., 1986; Zornberg et al., 1998b) have demonstrated that the likely range for the in-soil tensile strength value of nonwoven geotextile can be defined using wide-width and zero-span tensile tests. Thus, this study adopts the uniform distribution function for LE analyses.

4.2. Effect of orientation of reinforcement forces

The effect of reinforcement force orientation was investigated using LE analysis by assuming the reinforcement force acts at different orientations: horizontal (as-installed) to the failure surface, tangential (kinked along the shear surface) to the failure surface, and bisector of an angle between horizontal and tangential to the failure surface. The uniform distribution of reinforcement force with depth was adopted as mentioned previously. Table 4 summarizes the effect of reinforcement force orientation on the calculated T_{max} at wall failure in Tests S2, C4, and I12. Generally, the calculated T_{max} for the geotextile assumes to act tangentially is approximately 15% higher than other two assumed orientations. Notably, in Tests S2 and C4, T_{max} calculated by assuming tangential reinforcement force exceeds the T_{ult} value obtained from the zero-span test. These T_{max} values are questionable, as mentioned.

Fig. 10 shows the FSs for Test C4 calculated with increasing g-levels while considering different reinforcement force orientations. It can be observed in Fig. 10, the difference between calculated FSs is almost negligible. This calculation result can be explained as follows. The tangential reinforcement force produces a larger stabilizing moment than a horizontal force, but does not increase the normal forces (and consequently soil shear strength) along the shear surface. These two effects on system stability tend to compensate for each other. Consequently, the net effect of the selected reinforcement force orientation on the calculated FS is insignificant.

Fig. 11 shows the effect of reinforcement orientation on the predicted failure surface in Test C4. The assumed reinforcement force orientations in LE have marked effects on the location of the critical failure surface (Fig. 11). Generally, experimental and predicted locations of failure surfaces agree in analyses assuming horizontal and bisector reinforcement force orientations. The assumption of the tangential force orientation predicts a failure surface at a long distance from the wall face.

These analytical results for two-tiered walls are in agreement with the following findings from previous studies of GRS walls and slopes. Leshchinsky and Boedeker (1989) developed design charts for GRS structures using LE analyses by considering both horizontal and tangential reinforcement force orientations. The assumed horizontal reinforcement force produces a failure surface close to the slope/wall face. Zornberg et al. (1998b) parametrically evaluated the effect of reinforcement orientation on the calculated FS. The difference between FS calculated by assuming horizontal and tangential reinforcement force orientations was <10%. Additionally, Zornberg et al. (1998a) observed in-flight reinforced slope models with increasing g-levels and suggested that reinforcements remained horizontal until failure instead of tangential to the failure surface. Palmeira et al. (1998) verified that the assumption of reinforcement force acting horizontally in failure surfaces can produce satisfactory results in back analyses of geosynthetic reinforced embankments on soft soils. Overall, based on these numerical results and experimental evidence, geotextile strength acting horizontally to the failure surface is assumed for LE analysis.

5. Limit equilibrium results

After evaluating modeling assumptions, a series of LE analyses were performed to examine the validity of LE predictions for the failure of centrifuge two-tiered wall models with various offset distances. The LE results and design implications for multi-tiered GRS walls are presented.

5.1. Comparison of failure surface location

Fig. 12 compares locations of failure surfaces obtained experimentally from centrifuge tests and those predicted by LE analyses. The failure surface of the centrifuge wall model (black triangles in Fig. 12) was identified by tears (ruptures) in each reinforcement layer (Fig. 4). In most wall models (Fig. 12), the observed failure surfaces do not pass through the wall toe. The boundary constraint

Table 4
Effect of reinforcement force orientation on calculated T_{max} at wall failure.

Design	Test No.	D (mm)	T_{max} (kN/m)		
			Horizontal	Tangent	Bisector
Single	2	10	0.123	0.133	0.116
Compound	4	30	0.112	0.131	0.106
Independent (upper/lower)	12	270	0.076/0.066	0.094/0.074	0.072/0.062
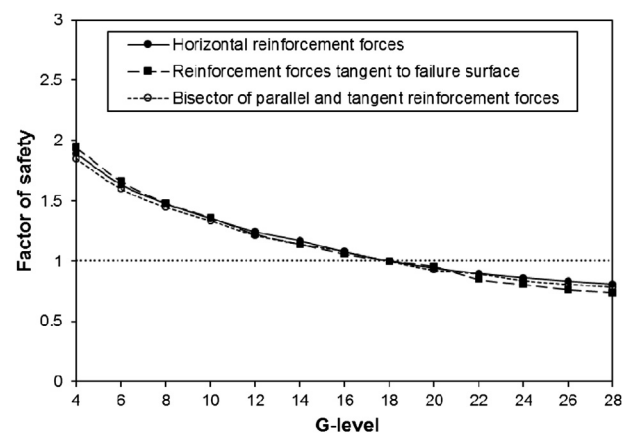
Fig. 10. Effect of reinforcement force orientation on calculated factor of safety for Test C4 with increasing g-level.
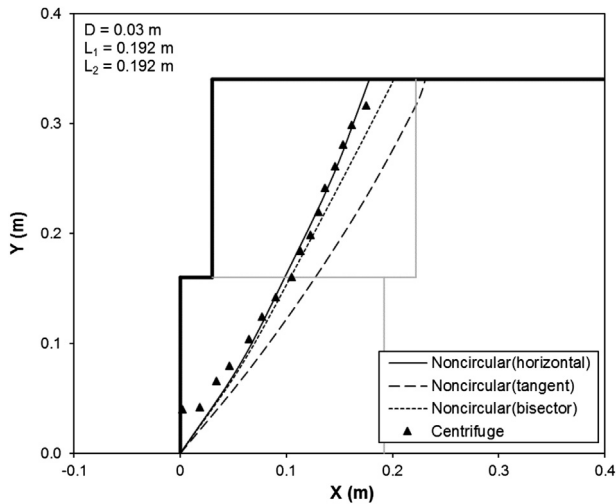
Fig. 11. Effect of reinforcement force orientation on predicted failure surface for Test C4.

from the dense and shallow foundation in centrifuge models likely prevented failure surfaces from passing through the wall toe. This firm foundation constrained soil movement, as well as reinforcement deformation, at wall base. Therefore, strains that develop in the bottommost reinforcement layer are too small to cause failure. Except for the difference between observed and predicted failure surfaces at the toe, comparison results (Fig. 12) indicate very good agreement between critical noncircular failure surfaces predicted by LE analyses and those experimentally observed for all wall models. The predicted locations of critical circular failure surfaces differ slightly from actual the locations of failure surfaces. Fig. 12 also compares experimental failure surfaces and maximum tension lines in FHWA design guidelines calculated using the procedure illustrated in Fig. 2a with $\phi_{tx} = 39.5°$ as the input value. In most cases, comparison results show that maximum tension lines in FHWA design guidelines depict the failure surfaces at a long distance from the wall face, particularly for the upper part of the upper tier. Therefore, using maximum tension lines recommended in FHWA design guidelines results in an overestimation of the required reinforcement embedment length, consequently leading to a conservative design against pullout.
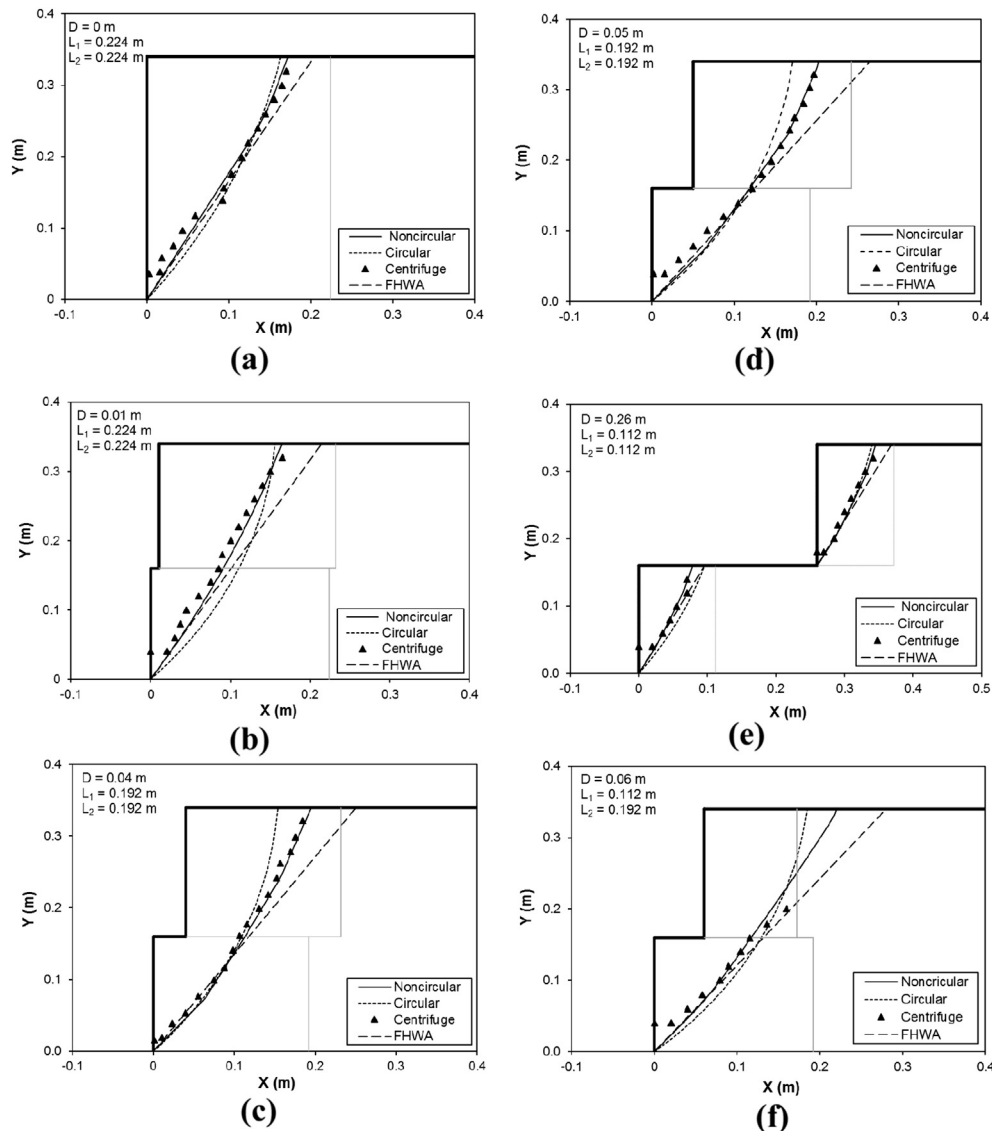

Fig. 12. Predicted and measured locations of failure surfaces from centrifuge tests: (a) Test S1; (b) Test S2; (c) Test C5; (d) Test C6; (e) Test I11; (f) Test SR14.

Moreover, four reduced-scale two-tiered GRS wall models with D varying at 0.10−0.4 m (Yoo et al., 2011) were also used for comparison in this study. Each reduced scale model was constructed by increasing its wall height until the wall failed under its own gravitational loading; the locations of failure surfaces of the four wall models were then determined. Fig. 13 shows comparison results. As has been proved, close agreement was obtained between measured and LE predicted failure surfaces. Although a clear difference between measured and LE predicted failure surfaces exists for the upper part of failure surfaces (Fig. 13a), the LE predicted failure surface agrees well with FE predicted failure surface in conjunction with the shear strength reduction method by Yoo et al. (2011). The results in Fig. 13 also show clear overestimations of failure surfaces obtained from the FHWA approach, particularly for the upper part of failure surfaces. Thus, the FHWA approach is conservative in its internal design against pullout.

Overall, LE analysis with a noncircular failure surface is superior to two other aforementioned methods (*i.e.*, LE analysis with a circular failure surface and maximum tension lines in FHWA design guidelines) in predicting the locations of failure surfaces of two-tiered walls. It can be concluded that the LE approach with a noncircular failure surface accurately predicts the failure surfaces of multi-tiered walls. Comparison results also support modeling assumptions (*e.g.*, use of the noncircular failure surface, uniform distribution of reinforcement forces with depth, and horizontal orientation of reinforcement forces) used in this study.

5.2. Effect of offset distance on confined T_{ult}

As mentioned, the ultimate tensile strength measured in the centrifuge test may differ from that measured in the standard unconfined tensile test due to soil confinement and impregnation of the geotextile by soil particles. One alternative is to evaluate in-soil geotextile strength by back-calculation from the centrifuge model results at failure. Table 1 summarizes calculated T_{ult} values which account for the average in-soil reinforcement tension at failure. Fig. 14 shows the effect of offset distance on the confined T_{ult}. For the I-series, only the confined T_{ult} values in the lower tier are presented. Clearly the confined T_{ult} value decreases as offset distance increases, and reaches a constant value beyond the critical offset distance D_{cr}. Analytical results imply that, as offset distance increases, the influence of the equivalent surcharge from the upper tier on reinforcements in the lower tier decreases, which then decreases the confined T_{ult}. The highest confined T_{ult} value was acquired from single walls because of their small offset distance, which induced a high overburden pressure on the reinforcement. Independent walls had the lowest confined T_{ult} values because the large offset distance decreased the overburden pressure from the upper tier acting on reinforcements in the lower tier. The unconfined T_{ult} values obtained by the wide-width and zero-span tests typically represent the potential range of confined T_{ult} values. The average confined T_{ult} value (about 0.119 kN/m) for single walls is very close to the T_{ult} value obtained from the zero-span test. The average confined T_{ult} value (about 0.07 kN/m) for independent walls is slightly larger than the T_{ult} value obtained from the wide-width test.

5.3. Determination of critical offset distance

Critical offset distance, D_{cr}, is defined as the offset distance beyond which two tiers act independently. In this study, $D_{cr} = 0.7H_2$ was identified when the decrease in the confined T_{ult} value as D increases reaches a constant value (the intersection of two trend lines in Fig. 14). Table 5 lists the critical offset distance, D_{cr}, reported
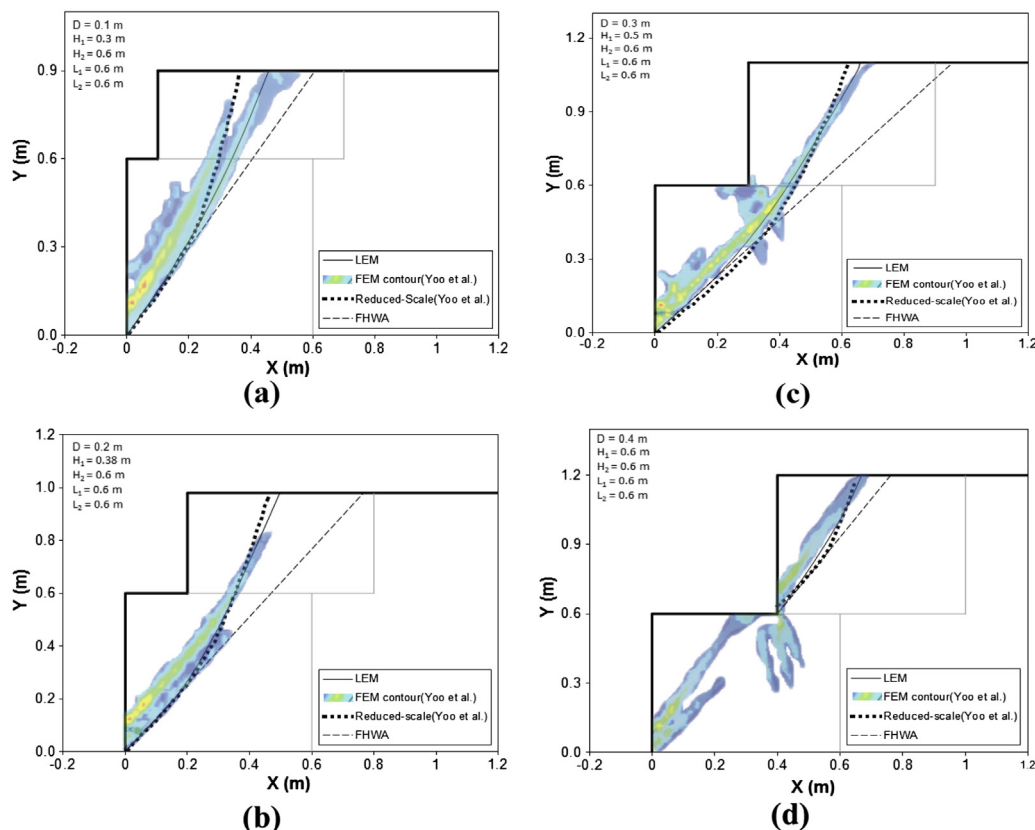

Fig. 13. Predicted and measured locations of failure surfaces from reduced-scale tests conducted by Yoo et al. (2011): (a) $D = 0.1$ m; (b) $D = 0.2$ m; (c) $D = 0.3$ m; (d) $D = 0.4$ m.
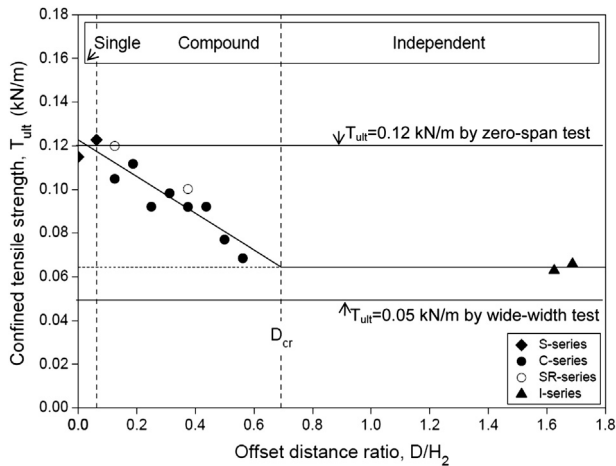
Fig. 14. Effect of offset distance on confined ultimate tensile strength.

by the design guidelines and previous studies. The small difference between D_{cr} in this study and D_{cr} (=0.8H_2) reported by Leshchinsky and Han (2004) and Yoo et al. (2011) may be attributed to the influence from backfill friction angle. Leshchinsky and Han (2004) showed that the D_{cr} value decreases from 1.2 to 0.8 as the value of the backfill friction angle increases from 25° to 43°. Generally, the D_{cr} determined in this study is in good agreement with the D_{cr} (=0.8H_2) reported by previous studies. However, the D_{cr} value determined in this study as well as those reported by previous studies is much less than the values recommended in FHWA and NCMA design guidelines. The D_{cr} value recommended by the FHWA is approximately 1.7 times greater than that determined in this study. Consequently, use of the D_{cr} value given in the current design guidelines would likely result in a conservative design.

5.4. Examination of methods to evaluate effective overburden pressure

The effective overburden pressures σ_v calculated using the FHWA approach and modified Gray's elastic solution are examined. The effective overburden pressure on the reinforcement then can be calculated as:

$$\sigma_v = \Delta\sigma_v + \sigma_z \tag{2}$$

where σ_v is the effective overburden pressure; $\Delta\sigma_v$ is the additional vertical stress from the upper tier; and σ_z is the overburden pressure from the lower tier. In the FHWA approach the additional vertical stress $\Delta\sigma_v$ (due to the influence of the equivalent surcharge from the upper tier) depends on D and H_1 as illustrated in Fig. 1b.

Table 5
Comparison of critical offset distances determined by various methods.

Current design approach and previous researches	Critical offset distance, D_{cr}	Method
FHWA (Elias et al., 2001; Berg et al., 2009)	$\tan(90° - \phi)H_2$ (=1.21H_2 with ϕ_{tx} = 39.5°)	Empirical
NCMA (2010)	L_2 for internal analysis, $L_2 + X_2$ for external analysis[a]	Empirical
Leshchinsky and Han (2004)	0.80H_2	Limit equilibrium
Yoo et al. (2011)	0.80H_2	Finite element
This study	0.70H_2	Limit equilibrium

[a] $X_2 = (H_2 + D/500)\tan\alpha$, where α is the inclination angle of the Coulomb failure surface, for tiered walls with vertical tiers and horizontal offset distances.

Gray (1936) proposed an elastic solution for estimating $\Delta\sigma_v$ in an elastic half-space subjected to an infinite overlying uniform loading (Fig. 15a).

$$\Delta\sigma_v = \frac{p}{\pi}\left(\beta + \frac{xz}{R^2}\right) \tag{3}$$

where $\Delta\sigma_v$ is the additional vertical stress, p is an infinite uniform load over half the surface, x and z are the horizontal and vertical distances from the origin of coordinates, and β and R are indicated in Fig. 15a. Wright (2005) modified Gray's elastic solution for estimating $\Delta\sigma_v$ of a multi-tiered "*flexible*" wall due to effect of overlying wall tiers (Fig. 15b and c). The $\Delta\sigma_v$ on a reinforcement layer at a given location (x, z) is defined by following equations:
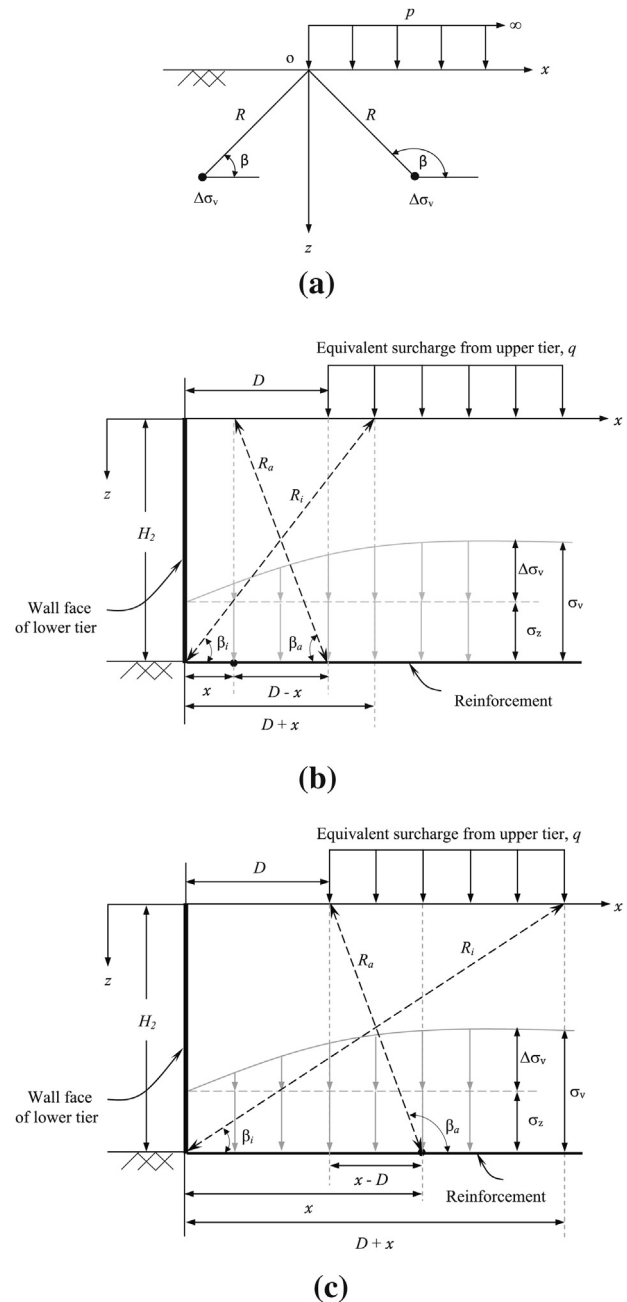

(a)

(b)

(c)

Fig. 15. Elastic vertical stress distributions: (a) Gray's solution (Gray, 1936); (b) and (c) modified Gray's solution proposed by Wright (2005) for a flexible walls when $x < D$ and $x \geq D$, respectively.

$$\Delta\sigma_v = \frac{q}{\pi}\left[\left(\beta_a + \frac{(x-D)z}{R_a^2}\right) - \left(\beta_i + \frac{(-x-D)z}{R_i^2}\right)\right] \qquad (4)$$

where q is the equivalent uniform surcharge from the upper tier, x is the horizontal distance from the wall face, D is the offset distance, z is the depth below the top of lower wall, and β_a, β_i, R_a and R_i are indicated in Fig. 15b and c and formularized as follows:

$$\beta_i = \tan^{-1}\left(\frac{z}{D+x}\right) \qquad (5)$$

$$\beta_a = \tan^{-1}\left(\frac{z}{D-x}\right) \quad \text{for } x < D \qquad (6a)$$

$$\beta_a = \pi + \tan^{-1}\left(\frac{z}{D-x}\right) \quad \text{for } x \geq D \qquad (6b)$$

$$R_i = \sqrt{z^2 + (D+x)^2} \qquad (7)$$

$$R_a = \sqrt{z^2 + (D-x)^2} \qquad (8)$$

Fig. 16 shows the results of evaluating the σ_v distribution along the 1st (bottom) and 4th reinforcement layers of the lower tier using the two approaches. The modified Gray's method produces preferable results: the calculated σ_v values increase as D decreases, which realistically reflects the increase in confined T_{ult} value as σ_v increases. The FHWA-recommended approach does not successfully represent the variation of σ_v with D. Fig. 16 shows negligible difference in σ_v calculated by FHWA approach for compound tests with various D values. It is because for the compound wall models with $(H_1 + H_2)/20 < D \leq \tan(45° - \phi/2)H_2$, the FHWA approach accounts for the full surcharge from the upper tier as the additional vertical stress in the lower tier (i.e., $\Delta\sigma_v = \gamma H_1$). Thus, the overburden pressure results obtained by the FHWA approach for walls with $(H_1 + H_2)/20 < D \leq \tan(45° - \phi/2)H_2$ are the same as that estimated for a single wall design, which may lead to an overestimated overburden pressure and, consequently, overdesign of reinforcements against rupture and a non-conservative design against pullout.

5.5. Effect of reinforcement length

The effect of reinforcement length was investigated by comparing the centrifuge test and LE results from the C- and SR-series. Long reinforcements ($L_1 = 0.6(H_1 + H_2) = 0.192$ m) were installed in the upper tier in the C-series while short reinforcements ($L_1 = 0.7H_1 = 0.112$ m) were used in SR-series. The measured and predicted locations of failure surfaces (Fig. 12c,d,f,) show that failure surfaces can pass through all reinforcement layers in C-series, while failure surfaces do not cut through almost half of the reinforcement layers in the upper tier in the SR-series. These analytical results imply that L_1 in SR-series, designed as the minimum required length ($L_{1,min} = 0.7H_1$) in FHWA design guidelines, is insufficient. As observed by Hung (2008), for reinforced walls with $(H_1 + H_2)/20 \leq D \leq (H_1 + H_2)/6.8$, designed as a compound wall in accordance to FHWA design guidelines, the instability of the upper tier likely occurs due to the insufficient L_1. As a result, both centrifuge test and LE results suggest that for the compound wall design, the minimum reinforcement length for the upper tier should be $L_{1,min} = 0.6(H_1 + H_2)$. Use of a longer minimum reinforcement length for the upper tier, $L_{1,min} = 1.25H_1$, in the compound wall design was also recommended by Yoo et al. (2011) based on FE studies of the effect of reinforcement length on
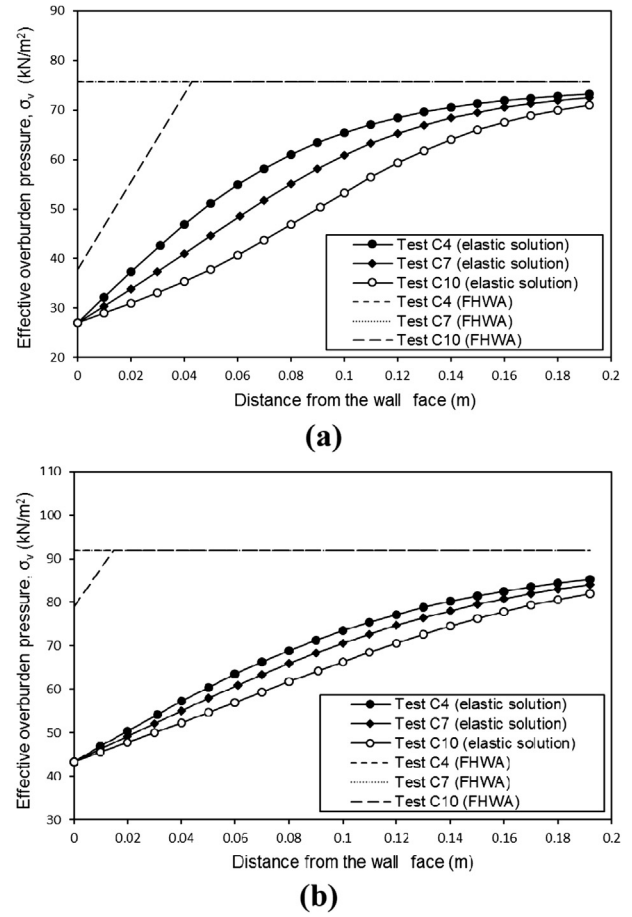

(a)

(b)

Fig. 16. Calculated σ_v distribution along reinforcement layers using FHWA approach and modified Gray's elastic solution: (a) the 4th layer; and (b) the 1st (bottom) layer.

maximum wall face displacement at FS = 1.2. Notably, the $L_{1,min}$ determined by Yoo et al. (2011) would be very close to the $L_{1,min}$ (=1.2H_1) recommended in this study when $H_1 \approx H_2$.

The effects of reinforcement length on failure g-levels and reinforcement confined T_{ult} are also examined. Table 1 shows that the failure g-levels in the SR-series are consistently 1 or 2 g less than those in the C-series with a given D. Although this difference in failure g-level is small, these comparison results reveal that parts of reinforcement layers in the upper tier in the SR-series are too short to be cut by the failure surface, such that the tensile strength of those reinforcements cannot contribute to system stability. Fig. 14 shows the effect of reinforcement length on calculated confined T_{ult}. The confined T_{ult} values in the SR-series follows the overall trend in Fig. 14 well, suggesting that the confined T_{ult} for a given reinforcement material is mainly influenced by the effective overburden pressure which is function of D and H_1 and slightly influenced by reinforcement length. Although the confined T_{ult} values are slightly larger than those in the C-series for wall models with the same D, this difference may be due to sensitivity of the calculated confined T_{ult} value for the failure g-level which is difficult to determine precisely at the moment of failure.

6. Normalization of reinforcement tension summations

In the LE analyses of two-tiered walls, equilibrium between reinforcement forces and horizontal soil stresses along the potential failure surface is essential. This equilibrium relationship can be

further characterized by an equivalent earth pressure coefficient, K_T, derived from the confined T_{ult}, defined as

$$K_T(\phi, \beta) = \left(\frac{2nT_{ult}}{\gamma H^2}\right) \cdot \frac{1}{N_f} \qquad (9)$$

where K_T is the equivalent earth pressure coefficient, so known as the normalized reinforcement tension summation coefficient at failure (Zornberg et al., 1998b). This coefficient K_T is function of the backfill friction angle ϕ and the configuration of two-tiered wall system (i.e., number of tiers and offset distance D) which can be represented as an equivalent wall inclination β; γ = unit weight of soil; H = total height of tiered walls; n = number of broken reinforcement layers (both primary and overlaps); T_{ult} = ultimate tensile strength of reinforcement back-calculated from the LE analysis; and N_f = failure g-level. When evaluating K_T using Eq. (9), only the tensile force of the broken reinforcement layers (i.e., nT_{ult}) is considered, assuming the mobilized tensile force in the unbroken reinforcements may be insignificant and can be omitted in the calculation.

Fig. 17 shows the normalized centrifuge test results. The linear relationship established for centrifuge models of single and independent walls (with the same ϕ and β). A single value of $K_T = 0.19$ is obtained. This K_T value is consistent with the value obtained from the Coulomb active earth pressure coefficient K_a for a vertical wall with a soil-facing interface friction angle of zero degree (i.e., $K_a = 0.195$). Fig. 17 also gives the normalization results for centrifuge models of compound walls (with the same ϕ but different β). The K_T value (the slope of the dashed line) decreases as offset distance D increases (or β decreases). These K_T values are further compared with those calculated using the Coulomb active earth pressure equation by inputting the corresponding β values. The comparison results in Fig. 18 indicate that the K_T values from compound wall models are slightly lower than those calculated by the Coulomb equation with different D or β values. This discrepancy between K_T and K_a is likely because soil-facing interface interaction occurred in the wall models is not considered accurately into the calculation of the Coulomb's K_a. Overall, good agreement between the K_T values and the Coulomb's K_a confirms that the predicted
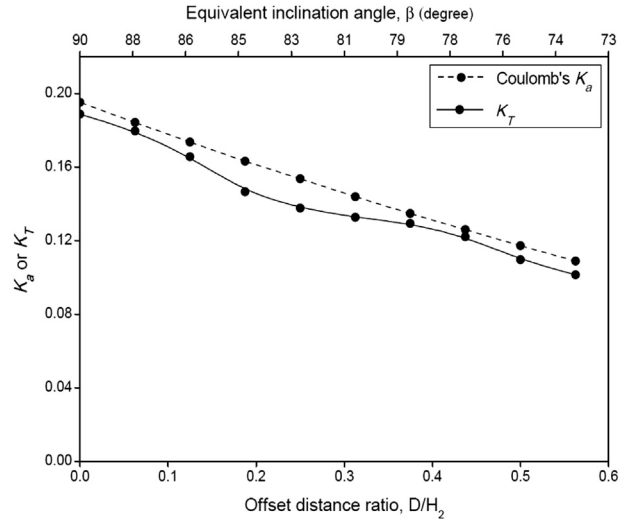

Fig. 18. Variation in normalized coefficient, K_T, obtained from centrifuge test results and K_a calculated from Coulomb equation with offset distance ratio.

confined T_{ult} values back-calculated from the LE analyses are reasonable and can be normalized as discussed in this section. Also, the Coulomb equation with the β value is capable of evaluating the equivalent earth pressure coefficients of two-tiered walls for internal stability design.

7. Conclusions

This study conducted a series of LE analyses for centrifuge modeling of two-tiered GRS walls with various offset distances. The effect of modeling assumptions of reinforcement force on the LE results and the validity of LE predictions on the failure of centrifuge two-tiered wall models were investigated. Details of the LE results and design implications for multi-tiered GRS walls were discussed. The conclusions drawn from this study are summarized below.

- The uniform tensile load distribution of reinforcements with depth and horizontal orientation of reinforcement forces are recommended for modeling reinforcement forces in LE analysis. The assumed tensile force distribution with depth has great effects on the max(T_{max}) value which typically used to determine long-term strength of reinforcements.
- The location of the critical noncircular failure surface predicted by LE analysis agrees well with the actual locations of the critical failure surfaces obtained experimentally. The maximum tension lines in FHWA design guidelines depict the failure surfaces at a long distance from the wall face, particularly for the upper part of the upper tier, resulting in an overestimation of the required reinforcement embedment lengths and consequently a conservative design against pullout.
- The centrifuge test results provide insight into the evaluation of the in-soil tensile strength of geotextile. The observed influence of offset distance, D, on the confined T_{ult} suggests that as offset distance increases, the effective overburden pressure acting on reinforcement decreases, which then decreases the confined T_{ult}. The modified Gray's elastic solution more realistically calculates the effective overburden pressure value as D increases compared to the approach suggested in FHWA design guidelines.
- The critical offset distance $D_{cr} = 0.7H_2$ was identified when the decrease in the confined T_{ult} value as D increases reaches a constant value. The D_{cr} value in this study agrees with those
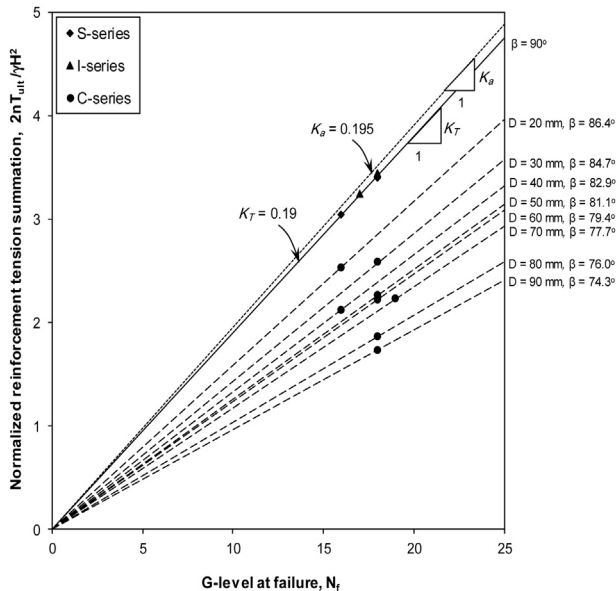

Fig. 17. Normalized reinforcement tension summation values from centrifuge test results.

reported in the previous studies and is much less than the values recommended in FHWA and NCMA design guidelines.

- The L_1 in SR-series, designed as the minimum required length ($L_{1,\min} = 0.7H_1$) in FHWA design guidelines, is insufficient, leading to parts of reinforcement layers in the upper tier cannot contribute to system stability and consequently wall models in SR-series fail earlier than those in C-series. As a result, for the compound wall design, the minimum reinforcement length for the upper tier $L_{1,\min} = 0.6(H_1 + H_2)$ is recommended.
- The normalization of the centrifuge test results obtains a consistent reinforcement tension summation coefficient K_T for single and independent walls (with the same ϕ and β). In compound wall models (with the same ϕ but different β), the K_T values, however, decrease as the offset distance D increases. The K_T values agreed with the Coulomb's K_a with varying β.

Finally, the limitations of this study are addressed as follows. First, the deformation of multi-tiered walls cannot be considered in the LE analyses conducted in this study. Second, although the effects of modeling assumptions for $T_{\max}$ on LE results have been extensively evaluated in the present study, these modeling assumptions require further verification using the results of finite element analyses or measured data from physical walls. Last, the findings and discussion in this paper are based on the centrifuge and LE results of two-tiered walls; further investigation is required for GRS walls with more than two tiers.

Acknowledgments

Notations

Basic SI units are given in parentheses

D	offset distance (m)
D_{cr}	critical offset distance (m)
$D_{T\max}$	distribution function (dimensionless)
FS	factor of safety (dimensionless)
H	height of two-tiered wall (m)
H_1	height of upper tier (m)
H_2	height of lower tier (m)
K_a	active earth pressure coefficient (dimensionless)
K_T	normalized reinforcement tension summation coefficient (dimensionless)
$K_T(\phi,\beta)$	equivalent earth pressure coefficient (dimensionless)
L_o	reinforcement overlap length (m)
L_1	reinforcement length of upper tier (m)
$L_{1,\min}$	minimum reinforcement length for the upper tier (m)
L_2	reinforcement length of lower tier (m)
$L_{2,\min}$	minimum reinforcement length for the lower tier (m)
$\max(T_{\max})$	maximum reinforcement load from all layers (kN/m)
n	number of reinforcement layers (dimensionless)
N_f	failure g-level of centrifuge model (dimensionless)
p	infinite uniform surcharge on a half elastic space (kN/m²)
q	equivalent uniform load from the upper tier (kN/m²)
$T_{\max}$	maximum reinforcement load in each layer (kN/m)
T_{ult}	confined ultimate tensile strength (kN/m)
x	distance from the wall face (m)
y/H	normalized elevation (dimensionless)
z	depth below the surcharge load (m)
β	equivalent wall inclination (degrees)
γ	unit weight of backfill soil (kN/m³)
θ	failure plane angle (degrees)
ϕ	friction angle of backfill (degrees)
ϕ_{ps}	plane strain peak friction angle (degrees)
ϕ_{tx}	triaxial compression test friction angle (degrees)
σ_z	overburden pressure at depth z (kN/m²)
σ_v	effective overburden pressures (kN/m²)
$\Delta\sigma_z$	additional vertical stress due to effect of overlying wall tier (kN/m²)

References

Allen, T.M., Bathurst, R.J., 2002. Soil reinforcement loads in geosynthetic walls at working stress conditions. Geosynth. Int. 9 (5–6), 525–566.

Allen, T.M., Bathurst, R.J., Holtz, R.D., Walters, D., Lee, W.F., 2003. A new working stress method for prediction of reinforcement loads in geosynthetic walls. Can. Geotech. J. 40 (5), 976–994.

ASTM, 1996. Standard test method for tensile properties of geotextiles by the wide-width strip method. ASTM D4595. In: Annual Book of ASTM Standards, vol. 4.09, pp. 698–708. West Conshohocken, PA.

Bathurst, R.J., Miyata, Y., Nernheim, A., Allen, T.M., 2008. Refinement of K-stiffness method for geosynthetic reinforced soil walls. Geosynth. Int. 15 (4), 269–295.

Boyle, S.R., Gallagher, M., Holtz, R.D., 1996. Influence of strain rate, specimen length and confinement in measured geotextile properties. Geosynth. Int. 3 (2), 205–225.

Berg, R., Christopher, B.R., Samtani, N., 2009. Design of Mechanically Stabilized Earth Walls and Reinforced Soil Slopes, vols. I and II. Federal Highway Administration, p. 684. Report No. FHWA-NHI-10-024.

Christopher, B.R., Holtz, R.D., Bell, W.D., 1986. New tests for determining the in-soil stress–strain properties of geotextiles. In: Proceedings of the Third International Conference on Geotextile, Vienna, Austria, pp. 683–686.

Elias, V., Christopher, B.R., Berg, R., 2001. Mechanically Stabilized Earth Walls and Reinforced Soil Slopes Design and Construction Guidelines. Report No. FHWA-NHI-00-043. National Highway Institute, Federal Highway Administration, Washington, D.C., USA, p. 418.

Gray, H., 1936. Stress distribution in elastic solids. In: Proceedings of Second International Conference on Soil Mechanics and Foundation Engineering, Cambridge, pp. 157–168.

Hung, W.Y., 2008. Breaking Failure Behavior and Internal Stability Analysis of Geosynthetic Reinforced Earth Walls (Ph.D. dissertation). National Central University, Jhongli, Taiwan, p. 200.

Jewell, R.A., 1991. Application of revised design charts for steep reinforced slopes. Geotext. Geomembr. 10 (3), 203–233.

Lade, P.V., Lee, K.L., 1976. Engineering Properties of Soils. Report UCLA-ENG-7652. University of California, Los Angeles, CA, p. 145.

Leshchinsky, D., Boedeker, R.H., 1989. Geosynthetic reinforced soil structures. J. Geotech. Eng., ASCE 115 (10), 1459–1478.

Leshchinsky, D., Han, J., 2004. Geosynthetic reinforced multitiered walls. J. Geotech. Geoenviron. Eng., ASCE 130 (12), 1225–1235.

Leshchinsky, D., Zhu, F., Meehan, C., 2010. Required unfactored strength of geosynthetic in reinforced earth structures. J. Geotech. Geoenviron. Eng., ASCE 136 (2), 281–289.

Liu, C.-N., Yang, K.-H., Ho, Y.-H., Chang, C.-M., 2012. Lessons learned from three failures on a high steep geogrid-reinforced slope. Geotext. Geomembr. 34 (0), 131–143.

Liu, H., 2011. Comparing the seismic responses of single- and multi-tiered geosynthetic reinforced soil walls. Geo-Frontiers 2011, 3478–3486.

NCMA, 2010. Design Manual for Segmental Retaining Walls, third ed. National Concrete Masonry Association, Herndon, Virginia, USA, p. 282.

Osborne, W.N., Wright, S.G., 2004. An Examination of Design Procedures for Single- and Multi-tier Mechanically Stabilized Earth Walls, p. 202. Report No. FHWA/TX-05/0-4485-1, Austin, Texas.

Palmeira, E.M., Pereira, Jose H.F., da Silva, Antonio R.L., 1998. Back analyses of geosynthetic reinforced embankments on soft soils. Geotext. Geomembr. 16 (5), 273–292.

Porbaha, A., Goodings, D.J., 1996. Centrifuge modeling of geotextile reinforced cohesive soil retaining walls. J. Geotech. Eng., ASCE 122 (10), 840–848.

Schmertmann, G.R., Chouery-Curtis, V.E., Johnson, R.D., Bonaparte, R., 1987. Design charts for geogrid-reinforced soil slopes. In: Proc., Geosynthetics 87 Can., New Orleans, La., pp. 108–120.

Spencer, E., 1967. A method of analysis of the stability of embankments assuming parallel inter-slice forces. Geotechnique 24 (4), 661–665.

Studlein, A.W., Bailey, M., Lindquist, D., Sankey, J., Neely, W.J., 2010. Design and performance of a 46-m-high MSE wall. J. Geotech. Geoenviron. Eng. 136 (6), 786–796.

Wright, S.G., 2005. Design Guidelines for Multi-tiered MSE Walls, p. 118. Report No. FHWA/TX-05/0-4485-2, Austin, Texas.

Yang, K.-H., Zornberg, J.G., Liu, C.-N., Lin, H.-D., 2012. Stress distribution and development within geosynthetic-reinforced soil slope. Geosynth. Int. 19 (1), 62–78.

Yoo, C., Jang, Y.S., Park, I.J., 2011. Internal stability of geosynthetic-reinforced soil walls in tiered configuration. Geosynth. Int. 18 (2), 74—83.

Yoo, C., Jung, H.S., 2004. Measured behavior of a geosynthetic reinforced segmental retaining wall in a tiered configuration. Geotext. Geomembr. 22 (5), 359—376.

Yoo, C., Kim, S.B., 2008. Performance of a two-tier geosynthetic reinforced segmental retaining wall under a surcharge load: full-scale load test and 3D finite element analysis. Geotext. Geomembr. 26 (6), 447—518.

Yoo, C., Song, A.R., 2007. Effect of foundation yielding on performance of two-tier geosynthetic reinforced segmental retaining walls: a numerical investigation. Geosynth. Int. 20 (3), 110—120.

Zornberg, J.G., Sitar, N., Mitchell, J.K., 1998a. Performance of geosynthetic reinforced slopes at failure. J. Geotech. Geoenviron. Eng., ASCE 124 (8), 670—683.

Zornberg, J.G., Sitar, N., Mitchell, J.K., 1998b. Limit equilibrium as basis for design of geosynthetic reinforced slopes. J. Geotech. Geoenviron. Eng., ASCE 124 (8), 684—698.